

14. Comparison Of The Effects Of Synthesis Methods Of B, N, S, And P-Doped Carbon Dots With High Photoluminescence Properties On Hela Tumor Cells

by Aswandi Wibrianto

Submission date: 09-Jun-2021 01:15PM (UTC+0800)

Submission ID: 1603264330

File name: s_With_High_Photoluminescence_Properties_On_Hela_Tumor_Cells.pdf (2.03M)

Word count: 7267

Character count: 36097


 Cite this: *RSC Adv.*, 2021, **11**, 1098

Comparison of the effects of synthesis methods of B, N, S, and P-doped carbon dots with high photoluminescence properties on HeLa tumor cells†

 Aswandi Wibrianto,^a Siti Q. Khairunisa,^b Satya C. W. Sakti,^{ac} Yatim L. Ni'mah,^d Bambang Purwanto^e and Mochamad Z. Fahmi^{id}*^{ac}

Although heteroatom doping is widely used to promote the optical properties of carbon dots for biological applications, the synthesis process still has problems such as multi-step process, complicating the setting of instrument along with uncontrolled products. In the present study, some elements such as boron, nitrogen, sulfur, and phosphor were intentionally doped into citric acid-based carbon dots by furnace- and microwave-assisted direct and simple carbonization processes. The process produced nanoparticles with an average diameter of 5–9 nm with heteroatoms (B, N, S, and P) placed on the core and surface of carbon dots. Among the doped carbon dots prepared, boron-doped carbon dots obtained by the microwave-assisted (B-CDs2) process showed the highest photoluminescence intensity with a quantum yield (QY) of about 32.96%. All obtained carbon dots exhibit good stability (at pH 6–12 and high ionic strength concentrations up to 0.5 M), whereas cytotoxicity analysis showed that all doped carbon dots are low-toxic with an average cell viability percentage above 80% up to 500 $\mu\text{g mL}^{-1}$. It can be observed from the CLSM image of all doped carbon dots that the doping process not only increases the QY percentage, but also might accelerate the HeLa uptake on it and produce strong carbon dot emission at the cytoplasm of the cell. Thus, the proposed synthesis process is promising for high-potency bioimaging of HeLa cancer cells.

 Received 5th November 2020
 Accepted 6th December 2020

DOI: 10.1039/d0ra09403j

rsc.li/rsc-advances

Introduction

Carbon-based nanomaterials have been widely used owing to their non-toxic attribute accompanied by the nanotechnology development on early cancer detection. Carbon dots (CDs) as a group of carbon nanomaterials have attracted much attention in the past few years due to their molecular size and

weight,¹ resistance to photobleaching and photodegradation,² excellent stability, high biocompatibility, and excellent low cytotoxicity compared to quantum dots and polymer dots.³ CDs can be synthesized from both synthetic and natural materials, such as citric acid, ascorbic acid, amino acids, glucose, and glycerol at high temperatures,⁴ via two common approaches, namely, the top-down method and the bottom-up method.⁵ The top-down method generally gives products with high yields but has many disadvantages including the complicating instrument, high cost, and uncontrollable morphology and size distribution of product yields.^{6,7} These limitations guide researchers to use the bottom-up method that was more promising with regard to size and shape.⁸ The bottom-up method consists of pyrolysis-based, template, chemical oxidation, thermal oxidation, reverse micelle and ultrasonic methods.⁶ One group of pyrolytic method, the carbonization based process through hydrothermal, microwave and ultrasonic methods has been mostly used. Although these methods yielded well-identified CDs, they still have disadvantages related to the complexity design, high cost and low luminescence intensity.^{9,10} Therefore, simple and low-cost strategies for overcoming these limitations need to be developed to intensify the optical properties of CDs.

^aDepartment of Chemistry, Universitas Airlangga, Surabaya 60115, Indonesia. E-mail: m.zakki.fahmi@fst.unair.ac.id; aswandi.wibrianto-2016@fst.unair.ac.id; satya.sakti@fst.unair.ac.id; Fax: +62-31-5922427; Tel: +62-31-5922427

^bInstitute of Tropical Disease, Universitas Airlangga, Surabaya 60115, Indonesia. E-mail: siti.qamariyah.khairunisa-2019@fk.unair.ac.id

^cSupramodification Nano-Micro Engineering Research Group, Universitas Airlangga, Surabaya 60115, Indonesia

^dDepartment of Chemistry, Faculty of Science and Data Analytics, Sepuluh Nopember Institute of Technology, Keputih, Sukolilo, Surabaya 60111, Indonesia. E-mail: yatimnikmah@gmail.com

^eDepartment of Medical Physiology, Faculty of Medicine Universitas Airlangga, Surabaya 601131, Indonesia. E-mail: bambang-purwanto@fk.unair.ac.id

† Electronic supplementary information (ESI) available: Image of doped CDs; molecular structure of pyrene; 3D conformation of AFM; XRD and XPS data of B-CDs2; stability images at varied pH and NaCl concentration; CC₅₀ plot of CDs2; CLSM image at varied incubation time; QY table; XPS composition table; and cytotoxicity table. See DOI: 10.1039/d0ra09403j



Furthermore, to enhance the fluorescence intensity of CDs, several efforts were made, one of them being the surface modification involving heteroatom doping. Doping is suitable to increase the quantum yield (QY) in CDs, as it can form n-type (extra electron) and p-type (extra-hole) carriers, even simultaneously, so that the electronic structure of CDs can be changed.¹ Several elements such as boron,^{11,12} nitrogen,¹³ sulphur,¹⁴ and phosphor were proposed as doping agents on CDs.¹⁵ Nitrogen- and sulphur-doped CDs were applied for the detection of Fe³⁺ ions and bioimaging.¹⁴ N-doped CDs (N-CDs) produce good visuals as excellent drug loading and delivery systems compared to the effects of cancer therapy such as chemotherapy.⁴ Boron, nitrogen, and sulphur doped into quantum dots (BNSQDs) produce a specific site in bioimaging cancer cells in the liver (HEPG2).¹⁶ Boron-doped carbon dots (B-CDs) can improve the nonlinear optical properties compared to carbon dots.¹⁷ Sulphur-doped carbon dots (S-CDs) are highly negatively charged particles because they contain sulphur and oxygen. This enables S-CDs to easily bind to the DNA-PEI complex. Therefore, S-CDs can be applied as bioimaging agents.¹⁸ Although there are many reports focusing on the nitrogen, boron, sulphur, and phosphor doping effects on CDs, the integrative evaluation and direct comparison studies of the effect of these elements on CDs applied as cancer staining agents are still limited. It will be a crucial aspect regarding the advantages promised by CDs.

Principally, the pyrolytic process accentuates carbonization that is first accompanied with dehydration of the CD source and prevents massive attraction of oxygen. This has made the pyrolytic method need a special set up as shown in hydrothermal, ultrasonic and microwave-assisted method. However, the way of minimizing the complicating design and simplifying the reaction step will be interesting to be discussed. In our previous work, we promoted the preparation of CDs via direct pyrolysis of the carbon source from both organic and commercial materials, which proved the effectiveness of the process and the excellent applicability of CDs.^{19–21} Motivated to prepare attractive doped CDs, in the present study, we report a strategy to simplify the synthesis of CDs with direct carbonization of citric acid and the doping source simultaneously. Commercial chemicals such as boric acid, nitric acid, sulphuric acid, and phosphoric acid were used as boron, nitrogen, sulphur and phosphor sources, respectively. For improved results, we used the carbonization process of CDs by giving furnace- and microwave-assisted treatments. Furthermore, the best doped CDs, based on their synthesis process, are applied as staining agents of HeLa cancer cells. This study utilized several characterization techniques including UV-Vis spectrophotometry, photoluminescence (PL), Fourier transform infra-red (FTIR) spectroscopy, X-ray diffraction (XRD), and atomic spectrum force microscopy (AFM). *In vitro* investigation to prove the cytotoxicity of CDs and its capability on HeLa markers was conducted by a CCK-8 assay along with confocal laser scanning microscopy (CLSM), indicating the potential use of CDs as HeLa staining agents.

Experimental

Materials

Citric acid (CA, 99.5%), boric acid (H₃BO₃), nitric acid (HNO₃, 65%), sulphuric acid (H₂SO₄, 95–97%), phosphoric acid (H₃PO₄, 85%), dimethyl sulfoxide (DMSO, 99.7%) and sodium hydroxide (NaOH) were purchased from Sigma-Aldrich (Germany). Ethanol (C₂H₅OH, 94–96%) was purchased from J. T. Baker (Malaysia). Hydrogen chloride (HCl, 37%) was purchased from Merck (Germany). Cell Counting Kit-8 (CCK-8), a cytotoxicity kit, was purchased from MedChemExpress (USA). All chemicals were used directly without further purification.

Synthesis of doping carbon dots by furnace- and microwave-assisted methods

The doped CDs were fabricated by following the latest work with some modifications.^{15,22,23} The bare CDs as well as boron-, nitrogen-, sulphur- and phosphor-doped CDs were prepared by combining citric acid (88.9 mg) with boric acid, nitric acid, sulphuric acid and phosphoric acid following the composition given in Table 1, respectively. For the furnace-assisted method, each mixture was calcined at 300 °C for 2 h in an isolated reactor. For the microwave-assisted method, the mixtures (following on Table 1) were placed into a microwave reaction system with 600 watt power and high temperature for 2 hours. For all samples, after the samples were naturally cooled down to room temperature, the dark brown CDs were obtained as a stacked precipitate on the bottom of the reactor. To prepare its colloidal solution, the doped CDs with adjusted concentration were first prepared by dissolving in a NaOH solution (0.1 M), and the pH was set at a neutral value. The solution was then further dialyzed on the membrane with a molecular weight cut off (MWCO) of 1 kDa to specify the CD size distribution and exclude the by-product.

Viability cell assessment

The cytotoxicity test of doped CDs was performed in HeLa cancer cells by a cell counting kit-8 (CCK-8) assay (MedChemExpress, New Jersey, USA). HeLa cell lines were first cultured at a density of 2.5×10^4 cells per well in a 96-well plate containing Dulbecco's modified Eagle's medium (DMEM) and

Table 1 Composition of the N-, B-, S-, and P-doped CDs

Sample ID	Method	Mol				
		CA	H ₃ BO ₃	HNO ₃	H ₂ SO ₄	H ₃ PO ₄
CDs1	Furnace-assisted	0.46	—	—	—	—
B-CDs1		0.46	0.2	—	—	—
N-CDs1		0.46	—	0.2	—	—
S-CDs1		0.46	—	—	0.2	—
P-CDs1		0.46	—	—	—	0.2
CDs2	Microwave-assisted	0.46	—	—	—	—
B-CDs2		0.46	0.2	—	—	—
N-CDs2		0.46	—	0.2	—	—
S-CDs2		0.46	—	—	0.2	—
P-CDs2		0.46	—	—	—	0.2



incubated for 24 h. Then, phosphate-buffered saline (PBS) was added to wash the cells. The cells were further incubated in 100 μL of DMEM with different concentrations of doped CDs (10 μL) for different durations. Once the adjusted time was reached, the reaction was continued by adding 1 mL of CCK-8 reagent (500 mg mL^{-1}) followed by incubation for 4 h. The absorbance of formazan on each plate correlated with the living cell was analyzed using a microplate reader at 450 nm. The cytotoxicity effects of doped carbon dots were assessed at half the cytotoxic concentration (CC_{50}) and fixed using the Origin software.

CLSM imaging assessment

For preparation, HeLa cells were cultured in a 6-well plate containing 2 mL Dulbecco's modified Eagle's medium (DMEM) and incubated for 24 hours. Each doped CD (400 μL) was further added and incubated for 1 h. The cells were then washed three times with PBS and fixed with 70% alcohol for about 10 min. Fluorescence images of doped carbon dots in HeLa cells were captured for immersion of 63×1.32 NA oil using confocal TCS SP2 (Leica Microsystems, USA) equipped with an inverted microscope and inline Ar (488 nm) and He-Ne (503–680 nm and 588 nm) laser.

Other characterizations

The synthesized products were characterized by several techniques. Fourier transform infra-red (FTIR) spectra were recorded using Infrared (IR) Tracer-100 (Shimadzu, Japan). Ultraviolet-visible (UV-Vis) spectra were recorded using a UV-Vis Shimadzu 1800 spectrophotometer (Shimadzu, Japan). The photoluminescence of doping carbon dots was collected using a LS 55 fluorescence spectrometer (Shimadzu, Japan). The PL of the doped CDs was determined comparatively by referring rhodamine 6G (R6G, QY (95%)); the % QY of doped CDs was calculated using the following equation:

$$\text{QY} = \text{QY}_{\text{R6G}}(I_{\text{CDs}}/I_{\text{R6G}})(A_{\text{CDs}}/A_{\text{R6G}})(\eta_{\text{water}}/\eta_{\text{ethanol}})^2$$

where I , A , and η are the integral PL intensity, UV absorbance and the optical density and refractive index of the solvent, respectively. Atomic force microscopic (AFM) images were acquired using a Nanoscan type AFM (Bruker, Germany).

In silico assessment

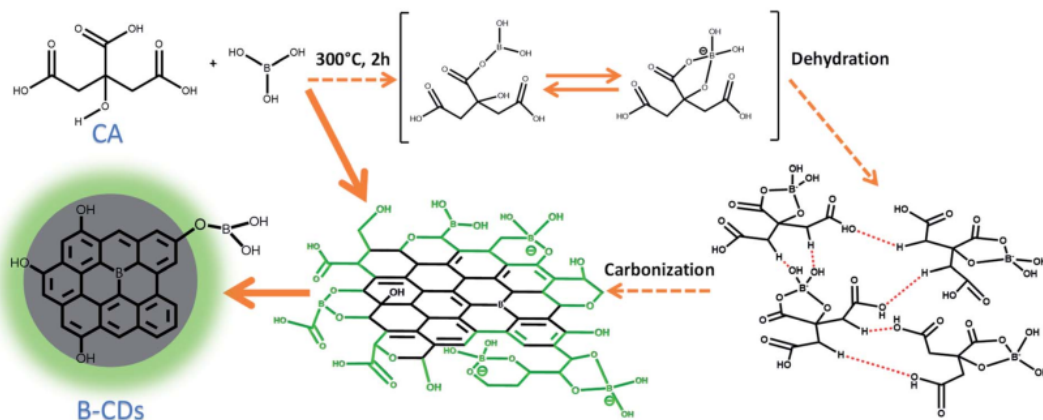
To represent all doped CDs with sp^2 and sp^3 features, we adopted pyrene-based systems with the doped elements and hydroxyl groups.^{24,25} The band gap was determined from the vertical electronic transition state data from each doped pyrene model that fully optimized using the density functional method with B3LYP²⁶ and orbital basis set at 6-31G + (d,p). The B3LYP/6-31G + (d,p) was chosen due to its proven capacity to generate the precise recurrence predictions.²⁷ The Hyper Chem 8.0 software program was used throughout this work.

Statistical analysis

The 50% cytotoxic concentration on cell viability (CC_{50}), was determined using the dose–response mode (nonlinear fitting) of the Origin software (version 8.0724, OriginLab Inc., Northampton, MA). All data were obtained in triplicate, with the simple t -test on some data.

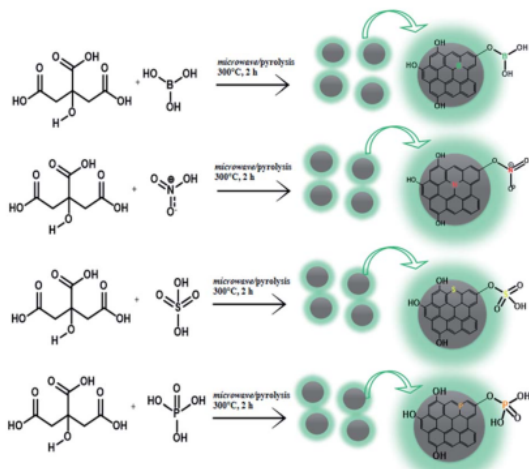
Results and discussion

The CDs were synthesized by simply treating citric acid with doping sources by a furnace and microwave-assisted method (Schemes 1 and 2). Basically, both methods were carried out over thermal treatment that allows dehydration and carbonization at low and high temperatures, respectively, which allows the rearrangement of the structure as well as its integration to form a graphene-like structure. However, this restructuring process is initiated by hydrogen bonds formed by doping with citric acid and between citric acids itself (as shown in Scheme 1).²⁸ Further carbonization will be performed for CDs with graphene oxide (GO) structures on some parts. The formation of CDs was proven by luminescence of those CDs under UV light



Scheme 1 Schematic on the mechanism of doped carbon dots (B-CDs).





Scheme 2 Schematic of the synthesis reaction of each doped carbon dot.

(Fig. S1, ESI†). This phenomenon came surely from electron's movement on the orbital state of CDs. However, the detailed mechanism of this fluorescence emission is still a subject of debate.

Besides size confinement and solvent effects, the emission of CDs mainly resulted from the synergic effects of confined sp^2 conjugation on the core of CDs and functional groups attributed on the surface of CDs.^{29,30} Thus, addition of different elements composing CDs will be an interesting aspect to be explored, also relating its consequence on the resulting band gap and adsorption-emission mechanism as well. To resolve these questions, we first investigated the absorption spectra of doped CDs (Fig. 1). By utilizing the furnace-assisted method, the maximum absorbance of bare CDs (CDs1) was founded at 226 nm with a shoulder peak at 289 nm. B-CDs1, N-CDs1, S-CDs1 and P-CDs1 have maximum absorbance at 228, 222, 224, and 222 nm, and the second absorption as shoulder peaks at 288, 288, 281, and 288 nm, respectively. Furthermore, the microwave-assisted method resulted in CDs2 with maximum absorbance at 229 nm wavelength with a shoulder peak at 322 nm (Fig. 1b) and doped B-CDs2, N-CDs2, S-CDs2 and P-CDs2 with maximum absorbance and shoulder peaks, respectively at 229 and 322 nm; 223 and 322 nm; 227 and 326 nm; 233 and 323 nm; 223 and 326 nm. From these data, the absorption band at wavelengths less than 300 nm indicates the $\pi-\pi^*$ transition of the conjugated C=C bond associated with a carbon core (carbogenic core). The absorption band at wavelengths over 300 nm signified the existence of $n-\pi^*$ transitions from C=O bonds or other groups such as NH_2 .³¹ Although maximum absorption and its shoulder peak are quite similar in each method, the adsorption peaks are relatively different in both furnace- and microwave-assisted methods. These bring a tendency that the furnace-assisted method will yield a particular structure of doped CDs that is different from that yielded by the microwave-assisted method. To prove this, we further use

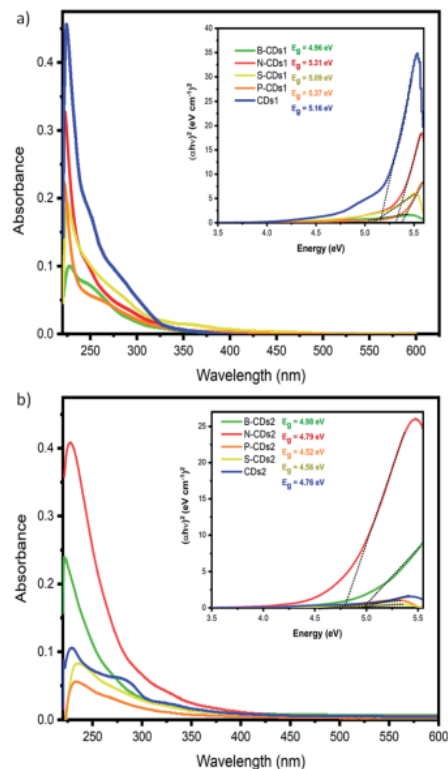


Fig. 1 UV-Vis spectra of doped carbon dots by (a) pyrolysis and (b) microwave-assisted methods. Inset: Tauc plot of each doped CD with its band gap measured.

the Tauc plot from the UV-Vis spectra data and find that the band gap values are varied (from 4.52 to 5.37 eV) depending on the doping and the method used (inset in Fig. 1). The sequence of the band gap in the furnace method is B-CDs1 < S-CDs1 < CDs1 < N-CDs1 < P-CDs1, while that in the microwave method is P-CDs2 < S-CDs2 < CDs2 < N-CDs2 < B-CDs2. These band gap differences are probably due to the complicating aspect to control the precise and homogenic structure of the proposed CDs. However, to get explanation for these phenomena, we further analogize proposed CDs with functionalized pyrene (Fig. S2, ESI†) and perform molecular modelling on pyrene to track the band gap that resulted with and without doping CDs (Fig. 2). The pyrene-based system was used for CD modelling based on the previous study. This computational modelling shows that the band gap energy of bare CDs and doped CDs follow a pattern in the microwave-assisted method, whereas B-CDs show the highest band gap compared with undoped CDs. These data indicated that the thermal induction from the microwave instrument can set carbonization, in which the position of doped atoms precisely matches with the proposed structure. In principle, microwave allows effective and fast heating of material *via* direct energy transfer and minimizes the dissipation of over-energy causing massive destruction that is common in the conventional heating process.³² Moreover, the



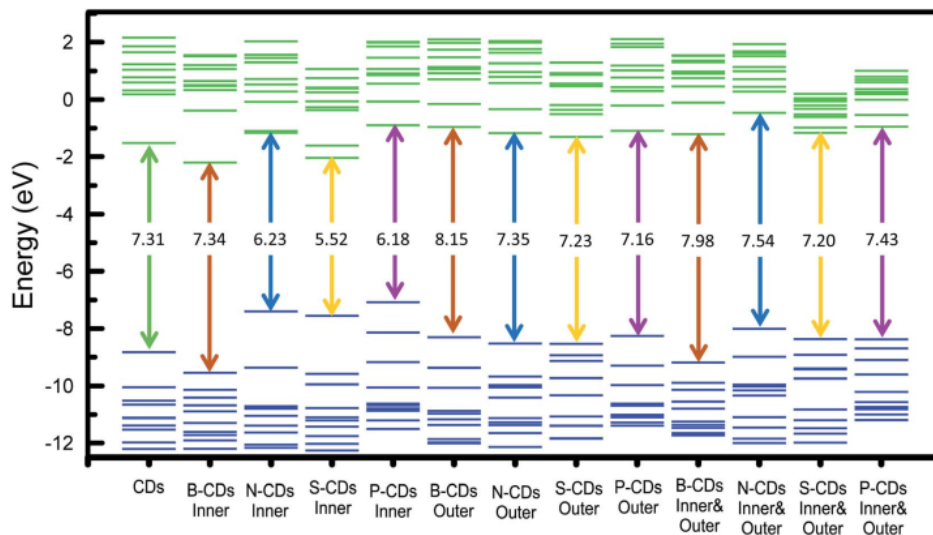


Fig. 2 Occupied (blue) and unoccupied (green) molecular orbitals of pyrene and doped pyrene as analogue structures of CDs and doped CDs, respectively. Energy level gap between HOMO and LUMO are described as double-line arrows with its energy value.

mechanism of heat transfer by the microwave treatment is considered by Joule heating from the conductive region of the π -system, which is the main part or any graphene-like structure including CDs; thus, this energy can accelerate and support effective carbonization to form CDs.³³ Furthermore, higher and lower band gaps on doped CDs are perhaps caused by doping type of proposed elements. Unlike boron, nitrogen, and phosphorus that mostly pretend as n-type, sulphur acts as a p-type upon CDs and other graphene-like structures, which is supposed to constrict the original band gap of CDs.^{34–36} Continuing on the optical properties investigation of doped CDs, we further evaluate the photoluminescence (PL) spectra of doped CDs1 (Fig. 3a–f) and doped CDs2 (Fig. 4a–f). With $\lambda_{\text{ex}} = 360$ nm, the emission fluorescence of all samples occurred at around 410–445 nm, which indicates strong blue fluorescence emission in aqueous solutions.³ The PL spectra also exhibit two overlapping peaks attributed to the π - π^* transition of C–C on the sp^2 domain of CDs (high electron transition) and the n - π^* transition as edge band transition of surface or doped groups (low electron transition). For most of the obtained CDs, the wavelength of emission (λ_{em}) shifted to a higher wavelength following the wavelength of excitation (λ_{ex}) exposure with a lower emission intensity. This excitation-dependent emission phenomenon commonly occurs in CDs by creating a new orbital trap known as the defect state due to the oxygenated group on CDs.^{37,38} It was well reported that all the doping elements have the potency to drive red-shift emission on a higher excitation wavelength;^{39,40} however, on B-CDs2 and N-CDs2, the PL spectra perform excitation-independent emission by wavelength maximum consistent at 455 nm (for λ_{ex} 360–400, Fig. 4b) and at 467 nm (for λ_{ex} 380–420, Fig. 4c), respectively. Among other doped CDs, carbon dot doped with H_3BO_3 by the microwave-assisted method (B-CDs2) shows the highest fluorescence

intensity. This is also indicated by the quantum yield (QY) value, in which the B-CDs2 value reaches 32.96%. For the quantum yield (QY) calculation, rhodamine 6G (R6G) was used as the reference (QY = 95%).⁴¹ Separately, the QY values for CDs1, B-CDs1, N-CDs1, S-CDs1, and P-CDs1 were sequentially 31.30%, 31.92%, 31.44%, 31.30%, and 31.37%; while for CDs2, N-CDs2,

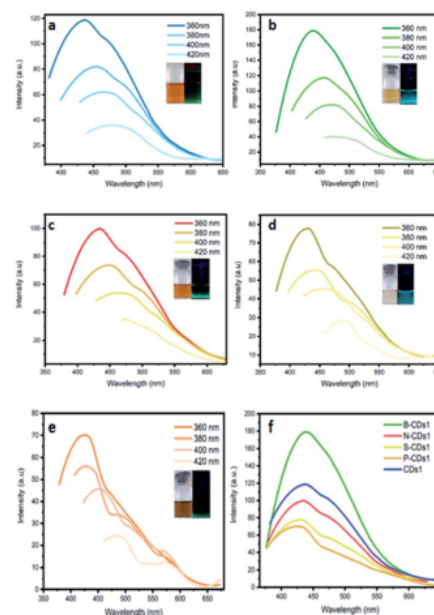


Fig. 3 PL spectra of (a) CDs1, (b) B-CDs1, (c) N-CDs1, (d) S-CDs1, and (e) P-CDs1 at varied λ_{ex} . (f) PL spectra of all CDs prepared by pyrolysis method at λ_{ex} 360 nm.



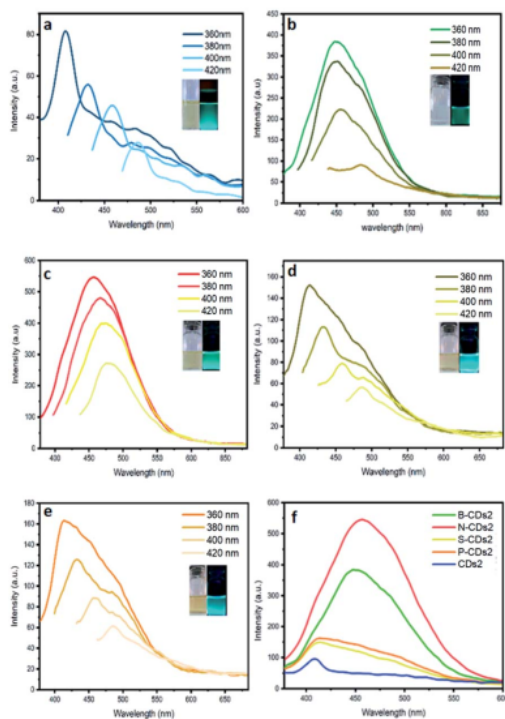


Fig. 4 PL spectra of (a) CDs2, (b) B-CDs2, (c) N-CDs2, (d) S-CDs2, and (e) P-CDs2 at varied λ_{ex} . (f) PL spectra of all CDs prepared by pyrolysis method at λ_{ex} 360 nm.

S-CDs2, and P-CDs2, the values were 31.17%, 32.49%, 32.59%, and 32.09%, respectively (Fig. 4). The QY data obtained for CDs are comparable with previous studies, which indicates good optical properties of CDs (Table S1, ESI[†]). Based on these data, it can be concluded that the application of a direct carbonization process through furnace and microwave treatment is favorable. Moreover, the addition of doping to CDs effectively enhances the emission intensity.⁴²

FTIR analysis was then carried out to confirm the functional groups produced on doped CDs (Fig. 5). All the prepared CDs have broad absorption peaks at 3638 to 3223 cm^{-1} , which are attributed to the stretching vibration of O–H and at 2959 cm^{-1} attributed to the stretching vibration of C–H of benzene.³⁸ Wavenumbers at 1738 to 1767 cm^{-1} verify the presence of a carbonyl group (C=O) of CA and the wavenumber at 1531 cm^{-1} from C=C groups of the benzene-like structure. Wavenumbers at 1207 to 1020 cm^{-1} confirm that there is a C–O group.³ The successful doping process into CDs was also revealed by CDs, where a stretching vibration at 1450 cm^{-1} indicates the presence of the B–O group,¹⁷ while C–N vibration give an FTIR signal at 1436 cm^{-1} .⁴³ The S=C vibration appears at 1075 cm^{-1} (ref. 44) and P–O–C vibration at 904 cm^{-1} .⁴⁵ All the above bands prove that the doping agents can be attached on CDs by both pyrolysis and the microwave-assisted synthesis process. Furthermore, a morphology study of CDs was performed by AFM demonstrating the distribution and particle

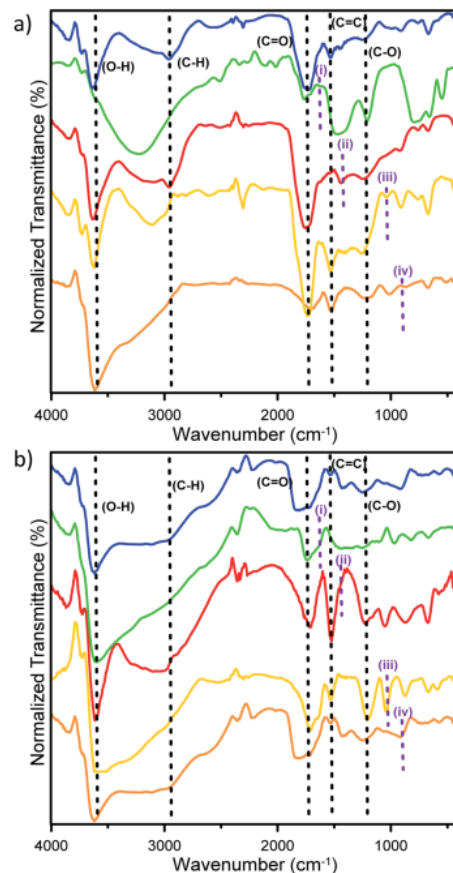


Fig. 5 IR data of doped carbon dots by (a) pyrolysis and (b) microwave-assisted methods, including CDs (blue line), B-CDs (Green line), N-CDs (red line), S-CDs (yellow line), and P-CDs (orange line). The particular purple-dot lines indicating B–O (i); C–N (ii); S=C (iii) and P–O–C (iv).

sizes of doped carbon dots (Fig. 6). Moreover, the 3D topography of each doped CD is shown in Fig. S3 (ESI[†]). From this figure, the pyrolysis treatments produce mostly small-sized CDs. For further improvement on AFM data, we use ImageJ software to adjust the size distribution of the obtained CDs, where B-CDs1, N-CDs1, S-CDs1, and P-CDs1 have the average diameter sizes of about 8.63, 7.47, 8.97, and 7.60 nm, respectively, and B-CDs2, N-CDs2, S-CDs2, and P-CDs2 have average diameter sizes around 9.35, 9.11, 8.06, and 5.04 nm, respectively. All of the doped carbon dots are classified as carbon dots owing to the diameter size below 10 nm with mostly spherical shape.^{5,46} The XRD analysis (Fig. S4a) (ESI[†]) showed broad (amorphous) peaks in the range of 2θ from 15° to 50°, which signified a carbon structure in the diffractogram of B-CDs2 samples. The amorphous peaks exhibited a graphitic crystal structure confirmed by JCPDS26-1076.¹² Sharp peaks at 27.77° indicated the presence of boron in the carbon dots, which was confirmed by JCPDS 06-0297.^{47–49}



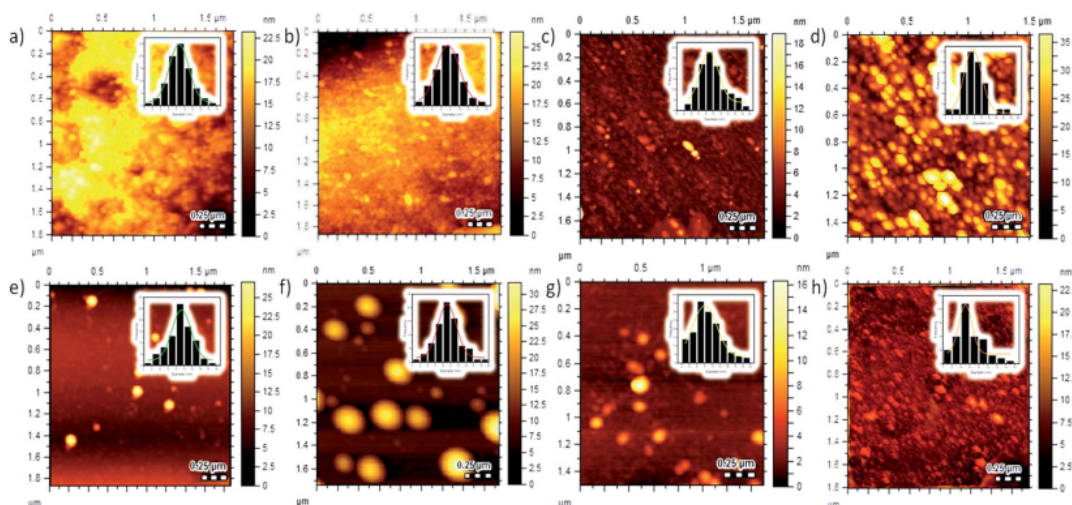


Fig. 6 AFM 2D topography images of (a) B-CDs1, (b) N-CDs1, (c) S-CDs1, (d) P-CDs1, (e) B-CDs2, (f) N-CDs2, (g) S-CDs2, and (h) P-CDs2. Inset: histogram data of distribution sizes.

B-CDs2 carbon dots were investigated even further by X-ray photoelectron spectroscopy (XPS) in order to acquire the existences of atoms including boron (B 1s), carbon (C 1s), and oxygen (O 1s) (Fig. S4b†). Table S2† shows the relative amount of carbon, oxygen, and boron, which were calculated as 56.85%, 39.63%, and 3.52%, respectively. The XPS C 1s spectrum is shown in Fig. S4d† displaying the presence of carbon signals at 285.1 (i) and 286.4 eV (ii), which indicated the existence of benzene and methoxy groups (C–O).⁵⁰ Then, the carbon spectrum at 289.6 eV (iii) clarified the presence of C=O (ester) of boric acid (H_3BO_3) conjugated to carbon dots.¹² High-resolution XPS shows O 1s spectra (Fig. S4e†) with peaks at 531.1 (iv), 532.2 (v), and 533.3 eV (vi), which were assigned to the presence of H–O, C–O, and B–O groups in carbon dot B-CDs2. Further measurements on the B 1s spectrum (Fig. S4e†) at 193.0 eV (vii) showed the presence of B–O groups in the sample.¹⁷

Stability evaluation of the doped-carbon dots

Colloidal stability analysis of the doped CDs was improved against different pH and NaCl concentrations (Fig. 7). This analysis is considered as stability data are important aspects for using nanomaterials in clinical applications. We first set doped CDs with a pH value ranging from 3 to 12 and observe that no precipitation nor agglomeration appeared by all of the doped pH (Fig. S5, ESI†). The stipulation of the pH range used in this investigation is based on the consistency of the pH value at intracellular areas of cells at pH 4.5 and pH 8 in the pancreas;⁵⁰ a previous study also reported that the optimal pH in the intracellular environment is from pH 4.5 to pH 7.5.¹⁵ However, B-CDs2 shows instability with significant precipitation at pH 3–4 and slight precipitation at pH 5 after 24 h, and it also happens in N-CDs2 at pH 3. These stability data toward the varying pH indicate that all of the doped CDs can be safely transferred at pH 6–12 to a human body without any harmful degradation.

Further, stability analysis was focused on the endurance of the CDs at different salt concentrations (from 0.1 M to 0.5 M), covering the normal ionic strength concentration (from 0.015 M to 0.14 M).⁵¹ Similar to its stability over pH, Fig. S6 (ESI†) proves that the doped CDs are quite resistant in facing the ionic effect of NaCl, even at high concentrations and over 24 h. To improve visual observation data of this stability, we next inspect the turbid value of each solution (Fig. 7). These considered as the colloidal system was once destructed, a precipitate would be produced and it could be tracked by increasing the turbidity level. The turbidity data on Fig. 7a inform its consistency with visual observation data, where all doped CDs perform good stability ($\leq 4,88$ NTU) on facing varied pH except pH 3–5 that is mostly greater than 6 NTU. The increasing of turbidity value on low pH condition occurred on all of the doped CDs. As well predicted before, CDs acts with abundant functional groups such as hydroxyl and carbonyl groups disposing as electronegative sites, forming hydrogen bonds intensely in an acidic atmosphere. This bonding will attract other CDs leading to CD accumulation and resulting in precipitate formation. However, the general turbidity of CDs on average is 4 to 5 NTU. Moreover, at different NaCl concentrations (Fig. 7b), all of the doped CDs show no significantly different turbidity level compared with the control (zero NaCl concentration). These data indicate that the doped CDs show good stability performance. This finding is supported by previous studies where the carbon dot modified at $MnFe_2O_4$ was stable at a salt concentration of 0.5 M.⁵⁰ Hence, all doped CDs have potential to be used in biomedical applications.

In vitro assessments

The simple synthesis and doping method proposed in this study was further directed to biomedical application by observing its capability in staining HeLa cancer cells. Although



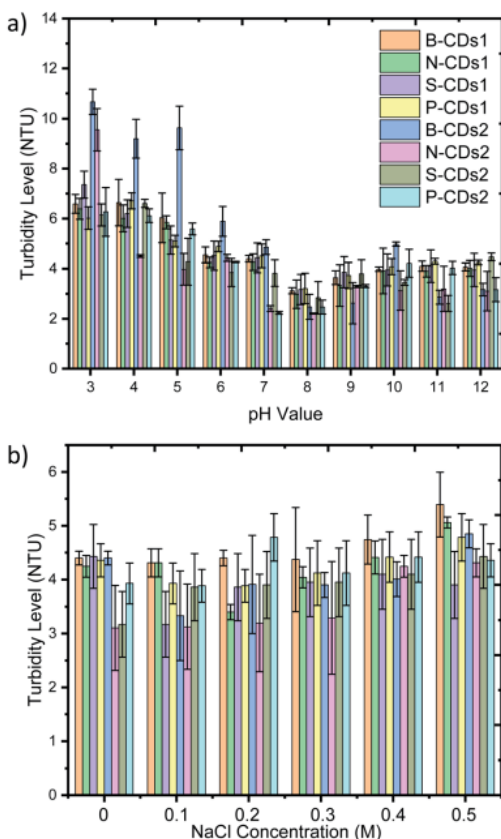


Fig. 7 Turbidity data of B-CDs1 (Orange); N-CDs1 (Bright Green); S-CDs1 (Purple); P-CDs1 (Yellow); B-CDs2 (Blue); N-CDs2 (Magenta); S-CDs2 (Green); P-CDs2 (Deep Sky Blue) at different (a) pH and (b) NaCl concentrations after 24 h. All data are expressed as mean \pm SD ($n = 3$).

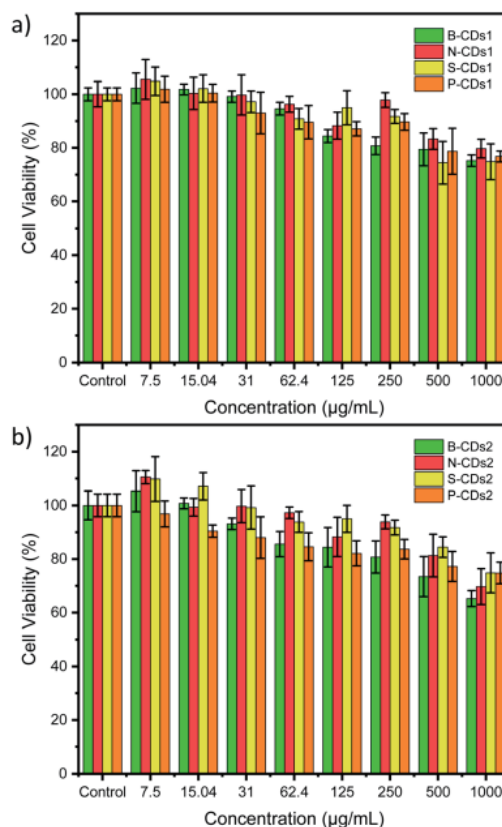


Fig. 8 HeLa cell viability data after 24 h incubation with different concentrations of furnace-assisted method-doped CDs1 (a) and microwave-assisted method-doped CDs1 (b). All data are expressed as mean \pm SD with $n = 3$.

boron doping on CDs was nominated as the best optical property (exhibit high % QY), the *in vitro* investigation on all of doped CDs are important to be revealed, due to comparable data. Cytotoxicity test by a CCK-8 assay was first carried out to discover the toxicity of the doped CDs. These methods use WST-8 or 2-(2-methoxy-4-nitrophenyl)-3-(4-nitrophenyl)-5-(2,4-disulfophenyl)-2H-tetrazolium monosodium salt, resulting in water-soluble formazan upon reduction process with mitochondrial dehydrogenases in living cells. Thus, the concentration of produced formazan is correlated with number of living cells. The CCK-8 results in Fig. 8 showed that the HeLa cell viability decreases with the increase in doped CD concentration after 24 h incubation. However, the viability was still greater than 80% on all doped CDs at 250 $\mu\text{g mL}^{-1}$, and it could first suggest the low-toxic property of doped CDs. Based on ISO 10993-5, the cell viability range of 120–80% indicates the low-toxic effects on cells.^{52,53} Improvements on these cytotoxicity data have been done by determining 50% cytotoxicity concentration (CC_{50}) of each doped CDs1 (Fig. 9) and CDs2 (Fig. S7, ESI†). The data shows that the CC_{50} of B-CDs1, N-CDs1, S-CDs1, P-CDs1, B-CDs2, N-CDs2, S-CDs2, and P-CDs2 are: 5289.15, 9217.56,

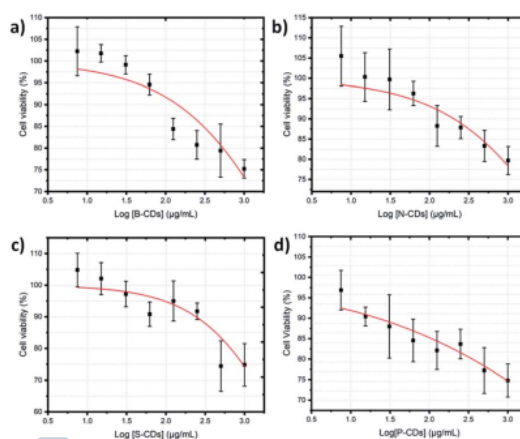


Fig. 9 Cell viability plot of HeLa cancer cells after 24 h incubation (a) B-CDs1, (b) N-CDs1, (c) S-CDs1, and (d) P-CDs1 by the microwave-assisted method. CC_{50} values were plotted on the red fitted curves that resulted from the dose response mode on the Origin software. All data are expressed as mean \pm SD with $n = 3$.



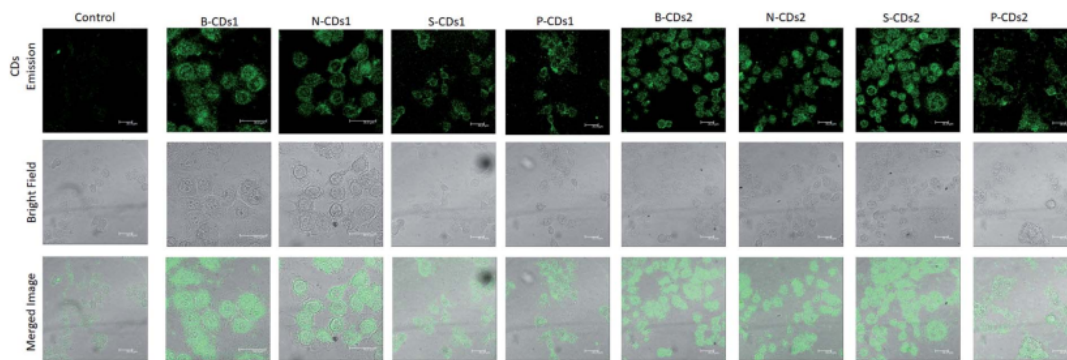


Fig. 10 Photograph CLSM images of HeLa cells after 1 h incubated without (control) and with the doped CDs by excitation at 488 nm. The scale bars represent 30 μm .

3725.18, 6710.52, 2444.72, 1945.04, 3218.58, and 40 318.13 $\mu\text{g mL}^{-1}$, respectively. The results, all over 1000 $\mu\text{g mL}^{-1}$, strongly indicated the low-toxic property on all doped CDs. The low-toxic statement in the present study can be recognized, while compared with other CDs reported from a previous study (Table S3, ESI†). Thus, all doped carbon dots are safe to be used in biological applications because these carbon dots have low toxicity in cells.

Further *in vitro* analysis was directed to discovering the capabilities of CDs as bioimaging agents using CLSM analysis. The CLSM results in Fig. 10 show that doped CDs can work well as HeLa markers compared with untreated cells (control). The figure also confirms that doped CDs can be effectively internalized to the cytoplasm of HeLa cells after 24 h incubation *via* the endocytosis process. To prove the entering mechanism, we captured the CLSM images of HeLa cells incubated with B-CDs1 for 10 min (Fig. S8, ESI†) that furnished low emission on the cell cytoplasm, whereas high emission on its membrane. These imply that the insertion of CDs occurred *via* the membrane-mediated endocytosis process. Although the cellular uptake of the doped CDs works through a passive targeting way (non-chemical interaction), the existence of boron elements allows the insertion of CDs *via* endocytosis mediated by sialic acid receptors overexpressing abundantly on the cell membrane of HeLa cells. Thus, it opens up the possibility of an active targeting process of CD cellular uptake, encouraging massive insertion as well as increased strong emission of the CDs in the cytoplasm of HeLa cells.⁵⁰ Moreover, it was previously reported that nitrogen, sulphur and phosphorus elements assist in the cellular uptake due to the emerging additional attraction of these elements with the cellular membrane.^{54,55} The CLSM results proved the above statements supporting that the doping elements encourage CDs to perform strong emission feature. Moreover, this finding indicates the good potential of the doped CDs to be applied on cancer cell staining agents.

Conclusions

In summary, carbon dots can be synthesized from citric acid by doping boron, nitrogen, sulphur, and phosphorus atoms by

a furnace- and microwave-assisted carbonization process. Several characterizations proved the successful doping of CDs, that is strengthened by *in silico* data. All doped CDs exhibited good colloidal stability, with the B-CDs2 compounds showing the highest optical property (QY value 32.96%), stable at pH 6–12 as well as ionic strength up to 0.5 M. The cytotoxicity assessment revealed that all the doped CDs are low-toxic with CC_{50} values on the upper grade comparing some previous study. The CLSM study showed the potential application of doped CDs as staining agents, and the doping elements on CDs facilitate the cellular uptake of CDs passing through the cellular membrane, thus performing significant CD emission in the cytoplasm.

Conflicts of interest

The authors declare no competing interest on present study.

Abbreviations

CDs	Carbon dots
QY	Quantum yield
CDs1	Furnace assisted carbon dots
CDs2	Microwave assisted carbon dots
B	Boron
N	Nitrogen
S	Sulphur
P	Phosphorus
UV-Vis	Ultra violet-visible
PL	Photoluminescence
FTIR	Fourier Transform Infra-Red
AFM	Atomic spectrum force microscope
CCK-8	Cell counting kit 8
CLSM	Confocal laser scanning microscope
CA	Citric acid
H_3BO_3	Boric acid
HNO_3	Nitric acid
H_2SO_4	Sulphuric acid
H_3PO_4	Phosphoric acid
DMSO	Dimethyl sulfoxide



Paper

NaOH	Sodium hydroxide
C ₂ H ₅ OH	Ethanol
DMEM	Dulbecco's Modified Eagle Medium
PBS	Phosphate-buffered saline
CC ₅₀	Cytotoxic concentration
R6G	Rhodamine 6G

35
Acknowledgements

The authors thank to Ministry of Research and Technology Republic of Indonesia Research support under contract No. 808/UN3.14/LT/2020 and Universitas Airlangga for Research Facilities.

References

- X. Zhang, J. Lu, X. Zhou, C. Guo and C. Wang, *Opt. Mater.*, 2017, **64**, 1–8.
- T. S. Atabaev, *Nanomaterials*, 2018, **8**, 342–351.
- X. Gao, Y. Lu, R. Zhang, S. He, J. Ju and M. Liu, *J. Mater. Chem. C*, 2015, **3**, 2302–2309.
- P. Gong, L. Sun, F. Wang, X. Liu, Z. Yan, M. Wang, L. Zhang, Z. Tian, Z. Liu and J. You, *Chem. Eng. J.*, 2018, **356**, 994–1002.
- M. Tuerhong, X. Yang and Y. Xue-bo, *Chin. J. Anal. Chem.*, 2017, **45**, 139–150.
- J. Wang and J. Qiu, *Journal of Materials Science*, 2016, **51**, 4728–4738.
- M. Semeniuk, Z. Yi, V. Poursorkhabi, J. Tjong, S. Jaffer, Z.-H. Lu and M. Sain, *ACS Nano*, 2019, **13**, 6224–6255.
- X. Dong, Y. Su, H. Geng, Z. Li, C. Yang, X. Li and Y. Zhang, *J. Mater. Chem. C*, 2014, **2**, 7477–7481.
- T. Ogi, H. Iwasaki, K. Aishima, F. Iskandar, W. N. Wang, K. Takimiya and K. Okuyama, *RSC Adv.*, 2014, **4**, 55709–55715.
- P. Shen, J. Gao, J. Cong, Z. Liu, C. Li and J. Yao, *ChemistrySelect*, 2016, **1**, 1314–1317.
- F. Wang, Q. Hao, Y. Zhang, Y. Xu and W. Lei, *Microchim. Acta*, 2016, **1**, 273–279.
- M. Z. Fahmi, W. Sukmayani, S. Q. Khairunisa, A. M. Witaningrum, D. W. Indriati, M. Q. Y. Matondang, J. Y. Chang, T. Kotaki and M. Kameoka, *RSC Adv.*, 2016, **6**, 92996–93002.
- F. Yarur, J.-r. Macairan and R. Naccache, *Environ. Sci.: Nano*, 2019, **6**, 1121–1130.
- C. Cheng, M. Xing and Q. Wu, *Mater. Sci. Eng., C*, 2019, **99**, 611–619.
- A. Pal, K. Ahmad, D. Dutta and A. Chattopadhyay, *ChemPhysChem*, 2019, **20**, 1018–1027.
- M. Pirsahab and S. Mohammadi, *Microchim. Acta*, 2019, **186**, 1–20.
- A. B. Bourlinos, G. Trivizas, M. A. Karakassides, M. Baikousi, A. Kouloumpis, D. Gournis and A. Bakandritsos, *Carbon*, 2014, **83**, 173–179.
- S. Chandra, P. Patra, S. H. Pathan, S. Roy, S. Mitra, A. Layek, R. Bhar, P. Pramanik and A. Goswami, *J. Mater. Chem. B*, 2013, **1**, 2375–2382.
- Y. Y. Aung, A. N. Kristanti, S. Q. Khairunisa, N. Nasronudin and M. Z. Fahmi, *ACS Biomater. Sci. Eng.*, 2020, 4490–4501.
- M. Z. Fahmi, D. L. N. Wibowo, S. C. W. Sakti and H. V. Lee, *Mater. Chem. Phys.*, 2020, **239**, 122266.
- M. Z. Fahmi, A. Haris, A. J. Permana, D. L. N. Wibowo, B. Purwanto, Y. L. Nikmah and A. Idris, *RSC Adv.*, 2018, **8**, 38376–38383.
- Y. Li, J. Bi, S. Liu, H. Wang, C. Yu, D. Li, B.-W. Zhu and M. Tan, *Food Funct.*, 2017, **8**, 2558–2565.
- X. Yang, Y. Zhuo, S. Zhu, Y. Luo, Y. Feng and Y. Dou, *Biosens. Bioelectron.*, 2014, **60**, 292–298.
- B. Shi, D. Nachtigallová, A. J. Aquino, F. B. Machado and H. Lischka, *Phys. Chem. Chem. Phys.*, 2019, **21**, 9077–9088.
- K. Hola, M. Sudolska, S. Kalytchuk, D. Nachtigalova, A. L. Rogach, M. Otyepka and R. Zboril, *ACS Nano*, 2017, **11**, 12402–12410.
- A. D. Becke, *J. Chem. Phys.*, 1993, **98**, 5648.
- C. Legler, N. Brown, R. Dunbar, M. Harness, K. Nguyen, O. Oyewole and W. Collier, *Spectrochim. Acta, Part A*, 2015, **145**, 15–24.
- M. Zhou, Z. Zhou, A. Gong, Y. Zhang and Q. Li, *Talanta*, 2015, **143**, 107–113.
- S. Zhu, Y. Song, X. Zhao, J. Shao, J. Zhang and B. Yang, *Nano Res.*, 2015, **8**, 355–381.
- C. Xia, S. Zhu, T. Feng, M. Yang and B. Yang, *Advanced Science*, 2019, **6**, 1901316.
- N. Dhenadhayalan, K.-c. Lin, R. Suresh and P. Ramamurthy, *J. Phys. Chem. C*, 2016, **120**, 1252–1261.
- T. Kim, J. Lee and K.-H. Lee, *Carbon Letters*, 2014, **15**, 15–24.
- E. Vazquez and M. Prato, *ACS Nano*, 2009, **3**, 3819–3824.
- M. Rastgoo and M. Fathipour, *Appl. Surf. Sci.*, 2019, **492**, 634–643.
- Y. Cao, H. Yu, J. Tan, F. Peng, H. Wang, J. Li, W. Zheng and N.-B. Wong, *Carbon*, 2013, **57**, 433–442.
- C. Liang, Y. Wang and T. Li, *Carbon*, 2015, **82**, 506–512.
- M. J. Krysmann, A. Kelarakis, P. Dallas and E. P. Giannelis, *J. Am. Chem. Soc.*, 2012, **134**, 747–750.
- Y. Deng, X. Chen, F. Wang, X. Zhang, D. Zhao and D. Shen, *Nanoscale*, 2014, **6**, 10388–10393.
- G. Yang, C. Wu, X. Luo, X. Liu, Y. Gao, P. Wu, C. Cai and S. S. Saavedra, *J. Phys. Chem. C*, 2018, **122**, 6483–6492.
- C. Wang, D. Sun, K. Zhuo, H. Zhang and J. Wang, *RSC Adv.*, 2014, **4**, 54060–54065.
- K. Lawson-wood, S. Upstone and K. Evans, in *Fluorescence Spectroscopy*, PerkinElmer Inc., Seer Green, UK, 2018.
- J. Zhou, H. Zhou, J. Tang, S. Deng, F. Yan and W. Li, *Microchim. Acta*, 2017, **184**, 343–368.
- R. Atchudan, T. N. J. I. Edison, S. Perumal, N. Karthik, D. Karthikeyan, M. Shanmugam and Y. R. Lee, *J. Photochem. Photobiol., A*, 2018, **350**, 75–85.
- J. Gliniak, J. H. Lin, Y. T. Chen, C. R. Li, E. J. J. Chang, C. S. Peng, J. N. Lin, W. H. Lien and H. M. Tsai, *ChemSusChem*, 2017, **10**, 3260–3267.
- H. Li, F.-Q. Shao, S.-Y. Zou, Q.-J. Yang, H. Huang, J.-J. Feng and A.-J. Wang, *Microchim. Acta*, 2016, **183**, 821–826.
- T. Pal, S. Mohiyuddin and G. Packirisamy, *ACS Omega*, 2018, **831–843**, 831–843.



- 47 Z. Fu and R. Koc, *Journal of the American Ceramic Society*, 2017, **100**, 2471–2481.
- 48 Y. Zhang, Y. Wang, C. Han, S. Jia, S. Zhou and J. Zang, *Nanoscale*, 2017, **9**, 19176–19182.
- 49 S. Kumar, S. Rajawat, R. Purohit and M. M. Malik, *Optik*, 2019, **176**, 617–625.
- 50 M. Z. Fahmi, J. K. Chen, C. C. Huang, Y. C. Ling and J.-Y. Chang, *J. Mater. Chem. B*, 2015, **3**, 5532–5543.
- 51 J. Dundas, G. Thickbroom and F. Mastaglia, *Clin. Neurophysiol.*, 2007, **118**, 1166–1170.
- 52 I. Iso, *Biological evaluation of medical devices—part 5: tests for in vitro cytotoxicity*, International Organization for Standardization, Geneva, 2009.
- 53 A. A. Ansari, T. N. Hasan, N. A. Syed, J. P. Labis and A. A. Alshatwi, *Saudi J. Biol. Sci.*, 2016, **24**, 1392–1403.
- 54 R. J. Brea and N. K. Devaraj, *Tension Promoted Sulfur Exchange for Cellular Delivery*, ACS Publications, 2017.
- 55 Q. Liu, Y. Qu, R. Van Antwerpen and N. Farrell, *Biochemistry*, 2006, **45**, 4248–4256.



14. Comparison Of The Effects Of Synthesis Methods Of B, N, S, And P-Doped Carbon Dots With High Photoluminescence Properties On Hela Tumor Cells

ORIGINALITY REPORT

16%

SIMILARITY INDEX

11%

INTERNET SOURCES

14%

PUBLICATIONS

0%

STUDENT PAPERS

PRIMARY SOURCES

1	Youfu Wang, Aiguo Hu. "Carbon quantum dots: synthesis, properties and applications", <i>Journal of Materials Chemistry C</i> , 2014 Publication	2%
2	en.wikipedia.org Internet Source	1%
3	Mochamad Zakki Fahmi, Denika Liyan Nor Wibowo, Satya Candra Wibawa Sakti, Hwei Voon Lee, Isnaeni. "Human serum albumin capsulated hydrophobic carbon nanodots as staining agent on HeLa tumor cell", <i>Materials Chemistry and Physics</i> , 2020 Publication	1%
4	pubs.rsc.org Internet Source	1%
5	researchonline.jcu.edu.au Internet Source	1%
6	www.molvis.org Internet Source	<1%

7 www.mdpi.com <1 %
Internet Source

8 M. Z. Fahmi, M. Wathoniyah, M. Khasanah, Y. Rahardjo, S. Wafiroh, Abdulloh Abdulloh. <1 %
"Incorporation of graphene oxide in polyethersulfone mixed matrix membranes to enhance hemodialysis membrane performance", RSC Advances, 2018
Publication

9 Velusamy Arul, Thomas Nesakumar Jebakumar Immanuel Edison, Yong Rok Lee, Mathur Gopalakrishnan Sethuraman. <1 %
"Biological and catalytic applications of green synthesized fluorescent N-doped carbon dots using *Hylocereus undatus*", Journal of Photochemistry and Photobiology B: Biology, 2017
Publication

10 www.ncbi.nlm.nih.gov <1 %
Internet Source

11 Chao Hu, Mingyu Li, Jieshan Qiu, Ya-Ping Sun. <1 %
"Design and fabrication of carbon dots for energy conversion and storage", Chemical Society Reviews, 2019
Publication

12 Huang, Hong, Ya-Chun Lu, Ai-Jun Wang, Jin-Hua Liu, Jian-Rong Chen, and Jiu-Ju Feng. "A <1 %

facile, green, and solvent-free route to nitrogen–sulfur-codoped fluorescent carbon nanoparticles for cellular imaging", RSC Advances, 2014.

Publication

13

doi.org
Internet Source

<1 %

14

www.insightsociety.org
Internet Source

<1 %

15

Baskar Thangaraj, Pravin Raj Solomon, Surawut Chuangchote, Nutthapon Wongyao, Werasak Surareungchai. "Biomass - derived Carbon Quantum Dots – A Review. Part 1: Preparation and Characterization", ChemBioEng Reviews, 2021

Publication

<1 %

16

Mochamad Zakki Fahmi, Roch Adi Prasetya, Muhammad Fathan Dzikri, Satya Candra Wibawa Sakti et al. "MnFe₂O₄ nanoparticles/cellulose acetate composite nanofiber for controllable release of naproxen", Materials Chemistry and Physics, 2020

Publication

<1 %

17

www.mysciencework.com
Internet Source

<1 %

18 Saheli Sarkar, Krishnendu Das, Moumita Ghosh, Prasanta Kumar Das. "Amino acid functionalized blue and phosphorous-doped green fluorescent carbon dots as bioimaging probe", RSC Advances, 2015
Publication

<1 %

19 Yang Yan, Longyu Xia, Lan Ma. "Solvent-controlled synthesis of multicolor photoluminescent carbon dots for bioimaging", RSC Advances, 2019
Publication

<1 %

20 Xi Wang, Tian Gao, Mian Yang, Jie Zhao, Feng-Lei Jiang, Yi Liu. " Microwave-assisted synthesis, characterization, cell imaging of fluorescent carbon dots using -asparagine as precursor ", New Journal of Chemistry, 2019
Publication

<1 %

21 thno.org
Internet Source

<1 %

22 www.tandfonline.com
Internet Source

<1 %

23 www.wjgnet.com
Internet Source

<1 %

24 Dan Wang, Xudong Wang, Yali Guo, Weisheng Liu, Wenwu Qin. "Luminescent properties of milk carbon dots and their sulphur and nitrogen doped analogues", RSC Adv., 2014

<1 %

25

Debabrata Ghosh Dastidar, Payel Mukherjee, Dipanjan Ghosh, Devdutt Banerjee. "Carbon quantum dots prepared from onion extract as fluorescence turn-on probes for selective estimation of Zn²⁺ in blood plasma", *Colloids and Surfaces A: Physicochemical and Engineering Aspects*, 2021

Publication

<1 %

26

Mochamad Zakki Fahmi, Keng-Liang Ou, Jem-Kun Chen, Ming-Hua Ho, Shin-Hwa Tzing, Jia-Yaw Chang. "Development of bovine serum albumin-modified hybrid nanoclusters for magnetofluorescence imaging and drug delivery", *RSC Adv.*, 2014

Publication

<1 %

27

Syamantak Khan, Akshita Sharma, Sourav Ghoshal, Sanjhal Jain, Montu K. Hazra, Chayan K. Nandi. "Small molecular organic nanocrystals resemble carbon nanodots in terms of their properties", *Chemical Science*, 2018

Publication

<1 %

28

bioone.org
Internet Source

<1 %

29

chemistrywithadoktor.blogspot.co.nz
Internet Source

<1 %

30

emboj.embopress.org

Internet Source

<1 %

31

livrepository.liverpool.ac.uk

Internet Source

<1 %

32

"Proceedings of the 1st International Conference on Electronics, Biomedical Engineering, and Health Informatics", Springer Science and Business Media LLC, 2021

Publication

<1 %

33

Jingran Bi, Yao Li, Haitao Wang, Yukun Song, Shuang Cong, Dongmei Li, Dayong Zhou, Bei-Wei Zhu, Mingqian Tan. "Physicochemical properties and cytotoxicity of carbon dots in grilled fish", New Journal of Chemistry, 2017

Publication

<1 %

34

Machado, Cláudia Emanuele, Letícia Gazola Tartuci, Honória de Fátima Gorgulho, Luiz Fernando Cappa de Oliveira, Jefferson Bettini, Daniela Pereira dos Santos, Jefferson Luis Ferrari, and Marco Antônio Schiavon. "Influence of Inert and Oxidizing Atmospheres on the Physical and Optical Properties of Luminescent Carbon Dots Prepared through Pyrolysis of a Model Molecule", Chemistry - A European Journal, 2016.

Publication

<1 %

35

Mochamad Zakki Fahmi, Jem-Kun Chen, Chih-Ching Huang, Yong-Chien Ling, Jia-Yaw Chang. "Phenylboronic acid-modified magnetic nanoparticles as a platform for carbon dot conjugation and doxorubicin delivery", Journal of Materials Chemistry B, 2015

Publication

<1 %

36

Paramita Karfa, Ekta Roy, Santanu Patra, Sunil Kumar, Abhrajyoti Tarafdar, Rashmi Madhuri, Prashant K. Sharma. " Retracted Article: Amino acid derived highly luminescent, heteroatom-doped carbon dots for label-free detection of Cd /Fe , cell imaging and enhanced antibacterial activity ", RSC Advances, 2015

Publication

<1 %

37

Raji Atchudan, Thomas Nesakumar Jebakumar Immanuel Edison, Dasagrandhi Chakradhar, Suguna Perumal, Jae-Jin Shim, Yong Rok Lee. "Facile green synthesis of nitrogen-doped carbon dots using Chionanthus retusus fruit extract and investigation of their suitability for metal ion sensing and biological applications", Sensors and Actuators B: Chemical, 2017

Publication

<1 %

38

Rui Zeng, Tingting He, Lu Lu, Ke Li, Zhong Luo, Kaiyong Cai. "Ultra-thin metal-organic

<1 %

framework nanosheets for chemo-
photodynamic synergistic therapy", Journal of
Materials Chemistry B, 2021

Publication

39

Yupeng Sun, Chen Shen, Jing Wang, Yun Lu.
"Facile synthesis of biocompatible N, S-doped
carbon dots for cell imaging and ion
detecting", RSC Advances, 2015

Publication

40

orca.cf.ac.uk

Internet Source

<1 %

41

s-space.snu.ac.kr

Internet Source

<1 %

42

www.hindawi.com

Internet Source

<1 %

43

www.scientific.net

Internet Source

<1 %

44

Du, Fengyi, Li Zhang, Lirong Zhang, Miaomiao
Zhang, Aihua Gong, Youwen Tan, Jiawen Miao,
Yuhua Gong, Mingzhong Sun, Huixiang Ju,
Chaoyang Wu, and Shenqiang Zou.

"Engineered gadolinium-doped carbon dots
for magnetic resonance imaging-guided
radiotherapy of tumors", Biomaterials, 2016.

Publication

<1 %

45

Jie Feng, Di Chang, Zhifei Wang, Bin Shen,
Jinjin Yang, Yanyun Jiang, Shenghong Ju,

<1 %

Nongyue He. "A FITC-doped silica coated gold nanocomposite for both in vivo X-ray CT and fluorescence dual modal imaging", RSC Adv., 2014

Publication

46

Mehbare Dogrusoz, Thomas Devic, Ali Şems Ahsen, Rezan Demir-Cakan. "A gallic acid based metal organic framework derived NiS/C anode for sodium ion batteries", Sustainable Energy & Fuels, 2021

Publication

47

Michal Langer, Markéta Paloncýová, Miroslav Medved', Martin Pykal et al. "Progress and challenges in understanding of photoluminescence properties of carbon dots based on theoretical computations", Applied Materials Today, 2021

Publication

48

Qianghua Ye, Fanyong Yan, Depeng Kong, Jin Zhang, Xuguang Zhou, Jinxia Xu, Li Chen. "Constructing a fluorescent probe for specific detection of catechol based on 4-carboxyphenylboronic acid-functionalized carbon dots", Sensors and Actuators B: Chemical, 2017

Publication

49

Qingyuan Niu, Kezheng Gao, Zhihui Lin, Wenhui Wu. "Amine-capped carbon dots as a

<1 %

<1 %

<1 %

<1 %

nanosensor for sensitive and selective detection of picric acid in aqueous solution via electrostatic interaction", *Analytical Methods*, 2013

Publication

50

Raji Atchudan, Thomas Nesakumar Jebakumar Immanuel Edison, Kanikkai Raja Aseer, Suguna Perumal, Yong Rok Lee.

"Hydrothermal conversion of *Magnolia liliiflora* into nitrogen-doped carbon dots as an effective turn-off fluorescence sensing, multi-colour cell imaging and fluorescent ink", *Colloids and Surfaces B: Biointerfaces*, 2018

Publication

51

Reza Tabaraki, Omran Abdi, Sedigheh Yousefipour. "Green and Selective Fluorescent Sensor for Detection of Sn (IV) and Mo (VI) Based on Boron and Nitrogen-Co-Doped Carbon Dots", *Journal of Fluorescence*, 2016

Publication

52

Shen, Juncai, Qing Li, Yan Zhang, Xing-jin She, Cai-Feng Wang, and Su Chen. "Nitrogen-doped carbon dots derived from polyamidoamine dendrimer", *RSC Advances*, 2016.

Publication

53

Syamantak Khan, Akshita Sharma, Sourav Ghoshal, Sanjhal Jain, Montu Hazra, Chayan

<1 %

<1 %

<1 %

<1 %

Kanti Nandi. "Small Molecular Organic Nanocrystals Resemble the Properties of Carbon Nanodots", Chem. Sci., 2017

Publication

54

Wenjing Lu, Xiaojuan Gong, Ming Nan, Yang Liu, Shaomin Shuang, Chuan Dong.

"Comparative study for N and S doped carbon dots: Synthesis, characterization and applications for Fe³⁺ probe and cellular imaging", Analytica Chimica Acta, 2015

Publication

<1 %

55

e-sciencecentral.org

Internet Source

<1 %

56

opus4.kobv.de

Internet Source

<1 %

57

www.dovepress.com

Internet Source

<1 %

58

www.google.com

Internet Source

<1 %

59

www.jmst.org

Internet Source

<1 %

60

Chunfeng Wang, Dong Sun, Yujuan Chen, Kelei Zhuo. " A hydrothermal route for synthesizing highly luminescent sulfur- and nitrogen-co-doped carbon dots as nanosensors for Hg ", RSC Advances, 2016

Publication

<1 %

61 Huang Zhou, Jian Zhang, Ibrahim Saana Amiinu, Chenyu Zhang, Xiaobo Liu, Wenmao Tu, Mu Pan, Shichun Mu. "Transforming waste biomass with an intrinsically porous network structure into porous nitrogen-doped graphene for highly efficient oxygen reduction", *Physical Chemistry Chemical Physics*, 2016

Publication

<1 %

62 Qingyan Zhang, Caihong Zhang, Zengbo Li, Jinyin Ge, Chenzhong Li, Chuan Dong, Shaomin Shuang. "Nitrogen-doped carbon dots as fluorescent probe for detection of curcumin based on the inner filter effect", *RSC Advances*, 2015

Publication

<1 %

63 Yu Yu Aung, Alfinda Novi Kristanti, Siti Qamariyah Khairunisa, Nasronudin Nasronudin, Mochamad Zakki Fahmi. "Inactivation of HIV-1 Infection through Integrative Blocking with Amino Phenylboronic Acid Attributed Carbon Dots", *ACS Biomaterials Science & Engineering*, 2020

Publication

<1 %

64 Myung Sun Lee. "Activation of AMP-activated protein kinase on human gastric cancer cells by apoptosis induced by corosolic acid

<1 %

isolated from Weigela subsessilis", Phytotherapy Research, 06/17/2010

Publication

Exclude quotes On

Exclude matches Off

Exclude bibliography On

14. Comparison Of The Effects Of Synthesis Methods Of B, N, S, And P-Doped Carbon Dots With High Photoluminescence Properties On Hela Tumor Cells

GRADEMARK REPORT

FINAL GRADE

/100

GENERAL COMMENTS

Instructor

PAGE 1

PAGE 2

PAGE 3

PAGE 4

PAGE 5

PAGE 6

PAGE 7

PAGE 8

PAGE 9

PAGE 10

PAGE 11
